Vanadium-modified titania-supported CuO-Fe$_2$O$_3$ systems and their efficiency in the Fenton-like degradation of phenol

Rania Ghanem, Yaser Yousef, Ayman Hammoudeh*

Chemistry Department, Yarmouk University, Irbid, Jordan, emails: ayman@yu.edu.jo (A. Hammoudeh), raniaghanem76@gmail.com (R. Ghanem), yhaj@yu.edu.jo (Y. Yousef)

ABSTRACT

A sol–gel method was adopted to prepare a series of titania-supported CuO-Fe$_2$O$_3$ systems modified by vanadium in various proportions (V$_2$O$_5$% ranging from 0%–25%). X-ray diffraction analysis showed that the pure TiO$_2$ system consists almost entirely of the anatase phase whereas all other titania supported systems are dominated by the rutile phase; small amounts of pseudobrookite (Fe$_2$TiO$_5$) and monoclinic CuO could also be identified. The former suggests the incorporation of Fe^{3+} in the TiO$_2$ lattice. In the case of the vanadium most-rich system in this work (25% V$_2$O$_5$), several extra diffraction features appear which could be attributed to the formation of various Cu(II) divanadate phases, the presence of which was also supported by infrared spectroscopy. Diffuse reflectance UV-Vis measurements were used to determine the band gap energies which lied in the range 1.86 eV–3.29 eV. Best performance in degrading phenol pollutant has been observed for the Fe$_2$O$_3$·CuO/TiO$_2$ system containing no vanadium, where almost total mineralization has been achieved. The catalytic performance was strongly enhanced by irradiation by a 23 W fluorescent lamp. Irradiation was also found to enhance the catalytic efficiency of the vanadium containing catalysts. The catalytic behavior was however suppressed by increased vanadium percentage, apparently due to the formation of vanadate phases.

Keywords: Pollution; Degradation; Fenton; Phenol; Irradiation; Catalysis; Iron(III) oxide; Titanium(IV) oxide

1. Introduction

Extensive research is being devoted to water pollution and its prevention as it represents a major challenge in modern civilization [1]. Several technologies have been applied to eliminate pollutants from wastewater; these include various chemical, physical and biological treatments [2]. Among these technologies, so-called advanced oxidation processes found a lot of attention as attractive and appealing alternatives because of the possibility to gain complete oxidation or mineralization of organic pollutants at or near ambient temperature and pressure with O$_3$, H$_2$O$_2$ and O$_2$ used as oxidizing agents [3]. The traditional homogenous Fenton reaction is catalyzed by Fe^{2+} ions and occurs generally at pH 2.0–4.0, with highest efficiency at pH 2.8–3.0 [4]. At pH higher than 4.0, the Fenton reaction slows down as a result of the precipitation of Fe^{3+} as Fe(OH)$_3$ [5]. Other drawbacks are the high cost of the process as well as the difficulties in recycling the catalyst. An elegant alternative is to use a solid catalyst which can be easily removed and reused at the end of the process. Moreover, the reaction efficiency can be enhanced by irradiation where the interest in replacing UV radiation by solar energy has increased in the past two decades [6]. Most of these used heterogeneous catalysts are iron oxides based. For repeated use, improvement of the mechanical properties of these catalysts has been attempted, for example by growing a Fe$_3$O$_4$/SiO$_2$ ceramic coating on a metal substrate [7].

---

* Corresponding author.

$CuFe_2O_4$ was used in the degradation of p-nitrophenol achieving almost 93% removal efficiency in 180 min [8]. $CuFe_2O_4$ synthesized via the sol-gel method was applied as a catalyst in the degradation of glycerol in aqueous solution where irradiation with visible light was reported to increase the glycerol degradation efficiency from less than 4.0% to nearly 40.0% [9]. $CuFe_2O_4$ prepared by the sol-gel auto-combustion method was compared with respect to its catalytic activity towards the degradation of phenol with that of $ZnFe_2O_4$ and $MgFe_2O_4$, as well as with a commercial TiO_2 catalyst. $CuFe_2O_4$ exhibited thereby the highest activity and it could be successfully regenerated and reused for five degradation cycles without a noticeable loss in its activity [10]. It was also reported that iron(II) doped copper ferrites, due to their favorable band-gap energies and peculiar structures, exhibit a strong potential for photocatalytic-degradation of dyes, for example, methylene blue [11].

Silver vanadates prepared by a microwave-assisted hydrothermal method showed strong visible-light absorption with energy gaps lying in the range 2.2–2.5 eV [12]. The α-Ag_3VO_4 crystalline sample rich in hydroxyl functional groups on the surface exhibited the highest photocatalytic activity, resulting under visible-light irradiation in photo-degradation rates for isopropanol and benzene vapors that are eight times higher than those over P25 TiO_2 [12]. In a recent study, six Fe-containing mixed oxide systems were prepared by means of the sol-gel auto-combustion method and tested as potential catalysts in the degradation of phenol. $CuFe_{1.2}O_{2.8}$ was thereby found to be the most reactive one showing an enhanced behavior under irradiation with a 30W LED light source. The enhancing effect of irradiation was strongest in the case of $Ag_2Fe_{5.4}V_3O_{16.6}$ where almost complete conversion was achieved in 120 min compared to only 45% in the absence of irradiation [13].

Aim of this work was to attempt to increase the phenol degradation efficiency of CuO-Fe_2O_3 systems by incorporating TiO_2 which is a widely investigated photocatalyst. Further modification by adding vanadium is also attempted. This work focuses on the effect of irradiation by a fluorescent lamp which represents a rather cheap source of radiation in the visible range.

2. Experimental

A series of titania-vanadia supported catalysts containing Fe_2O_3 and CuO were prepared through the sol-gel method using $Fe(NO_3)_3 \cdot 9H_2O$, $Cu(NO_3)_2 \cdot 3H_2O$, $C_{10}H_{14}O_5V$ (vanadyl acetylacetonate) and $Ti(OC_2H_5)_4$ (titanium(IV) tetraethoxide) as starting materials. Details can be found by the study of Ghanem [14], but in brief, appropriate amounts of $Cu(NO_3)_2 \cdot 3H_2O$, $Fe(NO_3)_3 \cdot 9H_2O$ and $C_{10}H_{14}O_5V$, based on the composition given in Table 1, were dissolved in 40 mL 96% ethanol (AZ); heating was applied to ensure complete dissolution of the added material. Then the required amount of $Ti(OC_2H_5)_4$ was added gradually while stirring until gel formation is complete. The gel was left overnight in oven at 120°C then calcined at 550°C under flowing oxygen (Arab Gas Company) for 4 h. Prepared catalytic systems are designated as $FxVy/TiO_2$ where the number y after vanadium (V) represents the mass percent of V_2O_5 in the system

and the number x is the summation of the percentage of CuO and Fe_2O_3 in the system.

The prepared catalysts were characterized with respect to their structure by means of X-ray diffraction (XRD), using a Shimadzu LabX device with a Cu-K_α–tube (λ = 1.5418 Å) in the range of 2θ = 15°–90° with a scanning rate of 0.5°/min. Vibrational properties and functional groups were investigated by infrared spectroscopy as KBr discs on a Bruker-FTIR Tensor 27 spectrometer in transmission mode. The electronic structure was characterized by diffuse reflectance UV-Vis spectroscopy (DRS) using a Shimadzu UV-2450 with ISR-2200 Integrating Sphere Attachment in the range of 200–800 nm with 1 nm slit width, and the BET surface area was determined on a Nova 2000 instrument by N_2 adsorption at 77.1 K and was found to be 80.4 m^2/g for $F20/TiO_2$.

To test the catalyst efficiency in the degradation of phenol, 0.25 g of the catalyst is added to 400 mL of 200 ppm phenol solution at 30°C in which a jacketed fluorescent lamp (Philips, 23 W, 1390 lm, CCT of 6500 K) has been immersed. The reaction progress was monitored for 5 h by high-performance liquid chromatography (HPLC; Dionex, Ultimate 3000 LC System, Chromelon Version 6.8) applying the following method: 250 × 4.6 mm C-18 column; mobile phase: 60% methanol and 40% water; flow rate: 1.200 mL/min; fixed wavelength detection at 270 nm.

The variation in the chemical oxygen demand (COD) throughout the reaction progress was also monitored applying the standard colorimetric closed-reflux method using commercial kits (WTW Germany GmbH), a Lovibond-RD 125 digester and a Lovibond-MD 100 photometer. The problem is that H_2O_2 present in the reaction solution interferes with the COD test as it reacts rather fast with $Cr_2O_7^{2-}$ reducing thus its concentration and leads to false COD readings. One way to overcome this difficulty is to determine the H_2O_2 concentration in the reaction sample and deduce then accordingly its contribution to the COD test. Iodometric titration is chosen to determine the concentration of H_2O_2.

3. Results and discussion

3.1. Catalyst characterization

3.1.1. X-ray diffraction

Fig. 1 shows the diffraction patterns of all seven systems in the range of 2θ = 23°–72°. For the sake of phase identification purposes, the stick patterns of reference phases have

Table 1
Supported catalysts investigated in this work

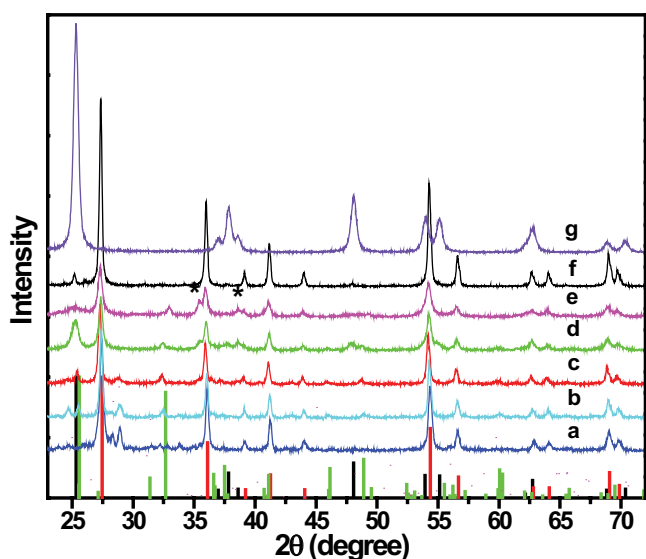| System	TiO_2%	CuO%	Fe_2O_3%	V_2O_5%
TiO_2	100	0	0	0
$V10/TiO_2$	90	0	0	10
$F20/TiO_2$	80	7	13	0
$F16-V5/TiO_2$	79	7	9	5
$F16-V10/TiO_2$	74	7	9	10
$F16-V15/TiO_2$	69	7	9	15
$F16-V25/TiO_2$	59	7	9	25

Fig. 1. X-ray diffraction patterns of (a) F16-V25/TiO$_2$, (b) F16-V15/TiO$_2$, (c) F16-V10/TiO$_2$, (d) F16-V5/TiO$_2$, (e) F20/TiO$_2$, (f) V10/TiO$_2$, and (g) TiO$_2$ (scanning rate 0.5°/min). Reference stick patterns for anatase (black), rutile (red) and pseudo-brookite (green) are included as vertical lines. Asterisks refer to monoclinic CuO.

been inserted in the figure as vertical lines. These correspond to anatase (black vertical lines, AMCSD 0019093), rutile (red vertical lines, AMCSD 0019092) and pseudobrookite (green vertical lines, AMCSD 0018179). The main conclusions drawn from the shown XRD patterns are presented:

- The TiO$_2$ system prepared in this work consists almost entirely of the anatase phase. This is consistent with literature reports that the anatase–rutile transformation below 600°C is very slow [15].
- When mixed with 10% V$_2$O$_5$ (pattern f in Fig. 1), the rutile phase becomes the dominant phase whereby the diffraction lines of anatase are strongly suppressed. This is also true for all other systems except F16-V5/TiO$_2$ where appreciable amounts of anatase are present, as evidenced especially by the diffraction line at ~25°. The enhancement of rutile formation at such rather a low temperature of 550°C, at which the calcination process was performed, can be attributed to the presence of iron and/or vanadium ions in the system.
- In the case of F20/TiO$_2$, the diffraction lines broaden with loss in intensity indicating poor crystallinity. In addition to the dominant rutile phase and small amounts of anatase, the presence of small amounts of pseudobrookite as well as monoclinic CuO (corresponding diffraction lines designated by asterisks according to the reference pattern JCPDS card 00-045-0937) can be identified. The formation of pseudobrookite indicates the incorporation of Fe^{3+} ions into the TiO$_2$ lattice. The fact that the diffraction features corresponding to pseudobrookite are rather small and the absence of the diffraction lines of any other Fe-containing system (α-Fe$_2$O$_3$, γ-Fe$_2$O$_3$, CuFe$_2$O$_4$ were checked for) suggest that most Fe^{3+} ions are dissolved in an amorphous state within the TiO$_2$

structure which is plausibly a pre-stage for the formation of pseudobrookite.

- Pseudobrookite is also present in all systems containing both Fe and V (patterns b–e in Fig. 1) except in the V most-rich system investigated in this work (F16-V25/TiO$_2$, pattern a), suggesting that in the presence of large amounts of vanadium, Fe^{3+} exists preferentially in a vanadate phase rather than in the pseudobrookite phase.
- In F16-V25/TiO$_2$, several extra diffraction features appear for example at 24.5, 28.5, 29 and 56°, which could be attributed to the formation of various Cu(II) divana-date and monovanadate phases: α-, β-, and γ-Cu$_2$V$_2$O$_7$ (AMCSD 0009530, 0014835 and 0006001, respectively), triclinic Cu$_3$(VO$_4$)$_2$ and Cu$_5$V$_2$O$_{10}$ (AMCSD 0009762 and 0009480, respectively). The formation of these Cu(II) vanadate phases explains also the disappearance of the diffraction lines of monoclinic CuO at high vanadium fractions.
- The crystallite size of all systems has been estimated by applying the Scherrer equation to the diffraction line at 44°:

$$d = \frac{K \cdot \lambda}{\beta \cdot \cos\theta} \qquad (1)$$

where K: Scherrer constant = 0.92; λ: Wavelength of applied X-ray (Cu-Kα1) = 1.54056 Å; θ: Diffraction angle; β: Line broadening due to decreased crystallite size in radians.

For all V-containing systems, the Scherrer crystallite size ranged from 61.5 nm for F16-V5/TiO$_2$ up to 77.0 nm for V10/TiO$_2$. On the other hand, F20/TiO$_2$ showed much broader diffraction bands corresponding to an estimated crystallite size of 33.8 nm.

3.1.2. Infrared spectroscopy

The infrared spectra are shown in Fig. 2 for all systems in the range 310–1,100 cm^{-1}. The range 1,100–4,000 cm^{-1} is not shown for clarity as it contains no characteristic bands of the oxide systems and only the broad band centered around 3,400 cm^{-1} corresponding to the O–H stretching vibration of adsorbed water as well as the associated H–O–H bending vibration at 1,640 cm^{-1} are observed in this range. The infrared spectrum f of TiO$_2$ with absorption extending to over 900 cm^{-1} is interpreted as a combination of the various transversal modes (TO) and longitudinal modes (LO) of the three infrared-active lattice vibrations of the anatase phase [16]. Incorporating V into TiO$_2$ (V10/TiO$_2$) led to a significant reduction in broadness of the strong absorption centered around 650 cm^{-1} (spectrum g). One possible explanation for this is that TiO$_2$ is now almost completely present in the form of rutile not anatase where the highest frequency in rutile is about 50 cm^{-1} smaller than that in anatase [17], accounting thus for the shorter range of absorption. Moreover, the two bands in spectrum g at 416 and 353 cm^{-1} agree with those of rutile, with that at 416 cm^{-1} being obviously a combination of the TO and LO modes at 381 and 443 cm^{-1}, respectively. Spectrum g shows also a small sharp band at 1,022 cm^{-1} corresponding to the stretching vibration of the vanadyl group (V=O).

The infrared spectra of the other systems are more complicated, for example by the presence of pseudobrookite and amorphous Fe–Ti–O phases in the case of F20/TiO$_2$ (Spectrum e in Fig. 2) and/or the presence of vanadate phases in the V-containing systems F16-V5/TiO$_2$, F16-V10/TiO$_2$, F16-V15/TiO$_2$ and F16-V25/TiO$_2$ (spectra d, c, b and a, respectively, in Fig. 2A). Analysis of the intensity change at selected wavenumbers as a function of the fraction of V$_2$O$_5$ is plotted in Fig. 2B. An abrupt increase in the band intensities at 640, 700, 830 and 937 cm^{-1} at V$_2$O$_5$ percentages above 10% is observed, which agrees well with the formation of vanadate phases at these percentages as evidenced by XRD. The band at 937 cm^{-1} is attributed to the VO$_3$ symmetric stretching

vibration while bands at 830 and 700 cm^{-1} are related to the VO$_3$ antisymmetric stretching vibrations [18].

3.1.3. Diffuse reflectance UV-Vis spectroscopy

Fig. 3a represents the UV-Vis diffuse reflectance spectra of TiO$_2$, V10/TiO$_2$ and F20/TiO$_2$. The reflectance spectra of the other systems are not shown for clarity purposes. TiO$_2$ shows a high reflectance (~90%) as expected for white materials. The reflectance drops however strongly due to absorption below 400 nm to reach only 2% at 350 nm. TiO$_2$ is a semiconductor with an energy gap of 3.0 eV for rutile and 3.2 eV for anatase [19]. This means that only radiation
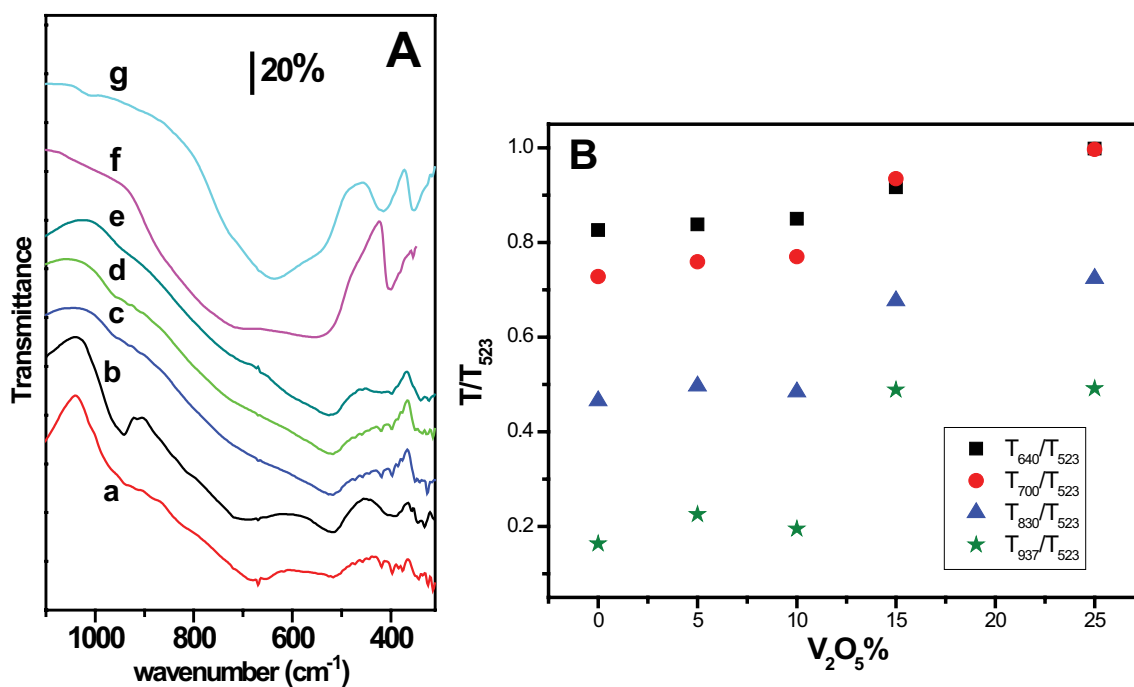

Fig. 2. (A) Infrared spectra (KBr discs, transmission mode) of the catalysts: (a) F16-V25/TiO$_2$, (b) F16-V15/TiO$_2$, (c) F16-V10/TiO$_2$, (d) F16-V5/TiO$_2$, (e) F20/TiO$_2$, (f) TiO$_2$ and (g) V10/TiO$_2$; (B) infrared transmission at 640, 700, 830 and 937 cm^{-1} relative to that at 523 cm^{-1} as a function of V$_2$O$_5$ percentage.
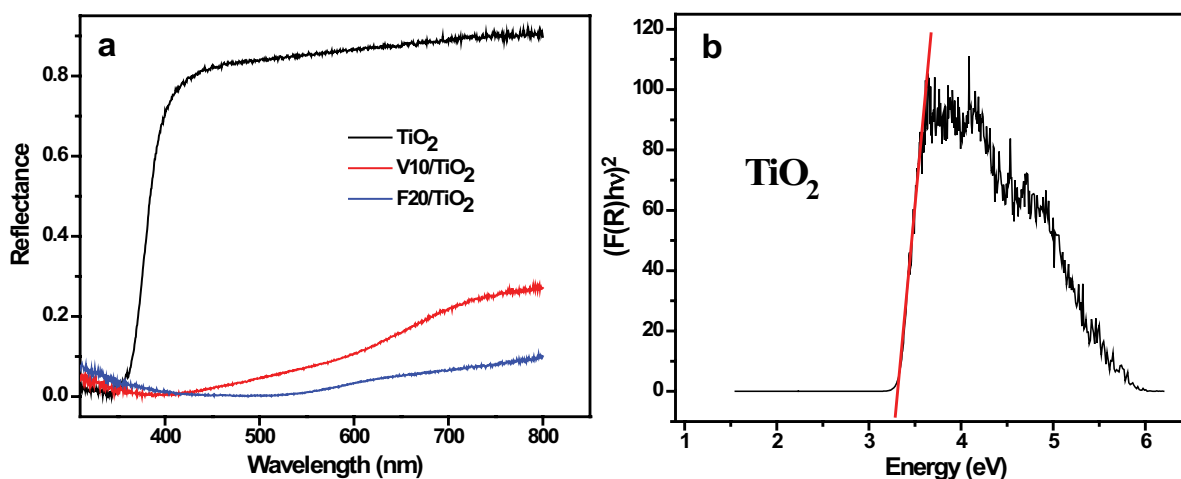

Fig. 3. (a) UV-Vis diffuse reflectance spectra of TiO$_2$, V10/TiO$_2$ and F20/TiO$_2$ and (b) Tauc's plot for TiO$_2$.

shorter than 413 nm in the case of rutile and shorter than 388 nm in the case of anatase is capable of being absorbed by these phases and provide the energy needed to transfer electrons from the valence band into the conduction band (the energy gap, E_g). E_g is often determined from the reflectance spectra of such materials through constructing the so-called Tauc's plot [20]. The absorption coefficient in the original Tauc's equation is thereby replaced by the Kubelka–Munk function $F(r_\infty)$ which describes the relation between the scattering and absorption characteristics and is given for samples of infinite thickness by $F(r_\infty) = (1 − r_\infty)^2/2r_\infty)$; r_∞ being the relative reflectance, that is, the reflectance of the sample relative to that of white non-absorbing reference material such as $BaSO_4$ or MgO. The Tauc's plot is shown in Fig. 3b for TiO_2. The intersect of the tangent at the point of inflection (red line in Fig. 3a) with the x-axis gives then an approximate value of the band gap in eV. Table 2 lists the experimentally determined values of the energy gap for the catalysts investigated in this work.

In Table 2, the band gap determined for TiO_2 is 3.29 eV which agrees well with that reported in literature to be 3.2 eV for anatase [19]. Incorporating vanadium (V10/TiO_2) reduces the band gap to 2.23 eV. Similarly, incorporating Fe^{3+} and Cu^{2+} (F20/TiO_2) reduces the band gap to 1.98 eV (For the sake of comparison, the gap energies for Fe_2O_3 and CuO are 2.0 eV [21] and 1.2 eV [22], respectively). After modification with vanadium, the band gap remains around 2 eV except for F16-V25/TiO_2 (the system with 25% V_2O_5) where it decreased further to 1.86 eV. Obviously, the presence of iron or vanadium is responsible for this significant reduction in the band gap energy compared to pure TiO_2.

3.2. Characteristics of light source

Fig. 4 shows the characteristic emission spectrum of the 23 W compact fluorescent lamp used in this work as a light source. The spectrum of the fluorescent lamp is broad and shows no radiation below 400 nm which can be attributed to the strong UV absorption of the glass bulb and the phosphor material that coats the inner surface of the bulb and acts as a UV-to-visible convector. Its emission is clearly shown in the intense line above 600 nm. The intense lines at 436 and 546 are the plasma emission lines of mercury while the low intensity lines before 600 nm are related to the mercury doublet at 576 and 579 nm. The low intensity of this lamp results from its rather low electric power.

Table 2
Experimental values for the band gap energies of investigated catalysts

Catalyst	Band gap (eV)
F20/TiO_2	1.98
F16-V5/TiO_2	1.96
F16-V10/TiO_2	2.02
F16-V15/TiO_2	1.97
F16-V25/TiO_2	1.86
V10/TiO_2	2.23
TiO_2	3.29

3.3. Phenol degradation

Fig. 5 represents an example of the obtained HPLC chromatograms, initially before the reaction starts (retention time t_R for phenol = 3.32 min) and after 300 min of reaction using F20/TiO_2 as a catalyst. The area of the phenol peak decreases with time, while various peaks appear at lower retention times (t_R = 1.68, 2.88, 2.13 and 2.64 min), corresponding to the formation of degradation intermediates. In general, the area of the intermediates peaks increases with time to some extent before decreasing again, as expected for intermediates in a consecutive reaction. Since complete mineralization is targeted, no attempt has been done in this work to identify the intermediates, the reason why their quantification was not possible. The absorption band at t_R = 2.3 min corresponds to residual H_2O_2 in solution.
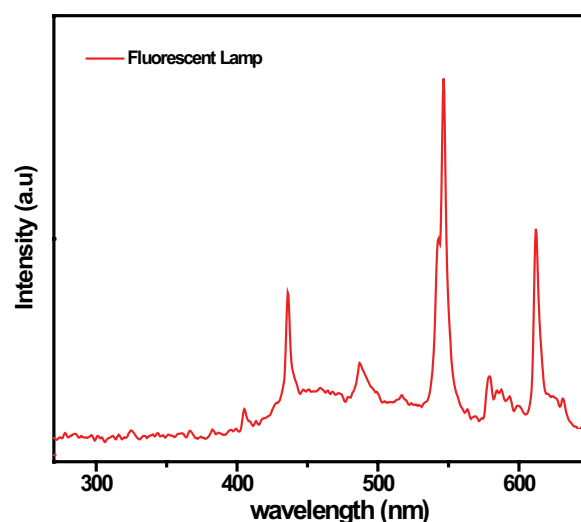

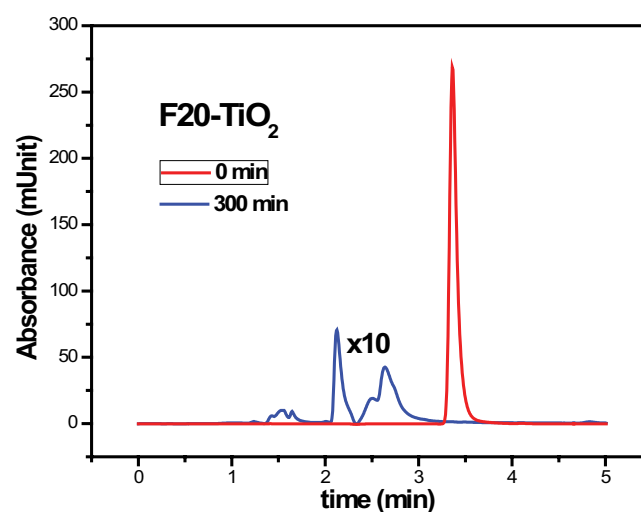Fig. 4. Characteristic emission spectra of the fluorescent lamp.

Fig. 5. HPLC chromatograms for zero time and after 300 min of reaction using F20/TiO_2 as a catalyst. Reaction conditions: 400 mL reaction solution with [phenol]$_o$ = 200 ppm and [H_2O_2]$_o$ = 0.0374 M, T = 30°C under irradiation with the jacketed 23 W fluorescent lamp.

Control experiments were performed to evaluate the extent of reaction in the absence of the catalyst (Fig. S1). The reaction was studied without as well as with irradiation with the fluorescent lamp. In the case of no irradiation, the degradation of phenol was limited, and the concentration of phenol drops from 200 ppm initially to only 184 ppm after 180 min of reaction. On the other hand, irradiation with the fluorescent lamp leads to 40 ppm of phenol remaining after 180 min of reaction. The difference in the two cases is attributed to the different rates of formation of the hydroxyl radicals. Whereas in the case of no irradiation only limited amounts of the reactive hydroxyl radicals are thermally produced, obviously much larger amounts are photolytically produced in the case of irradiation with the fluorescent lamp.

The catalytic behavior of $F20/TiO_2$ is depicted in Fig. 6 for the case of irradiation with the fluorescent lamp as well as in absence of irradiation. In both cases, the phenol concentration was found to decrease rather fast with time, exceeding, after 120 min of reaction in absence of irradiation, 96%-conversion of phenol and reaching, under irradiation, 100% conversion in the same time interval.
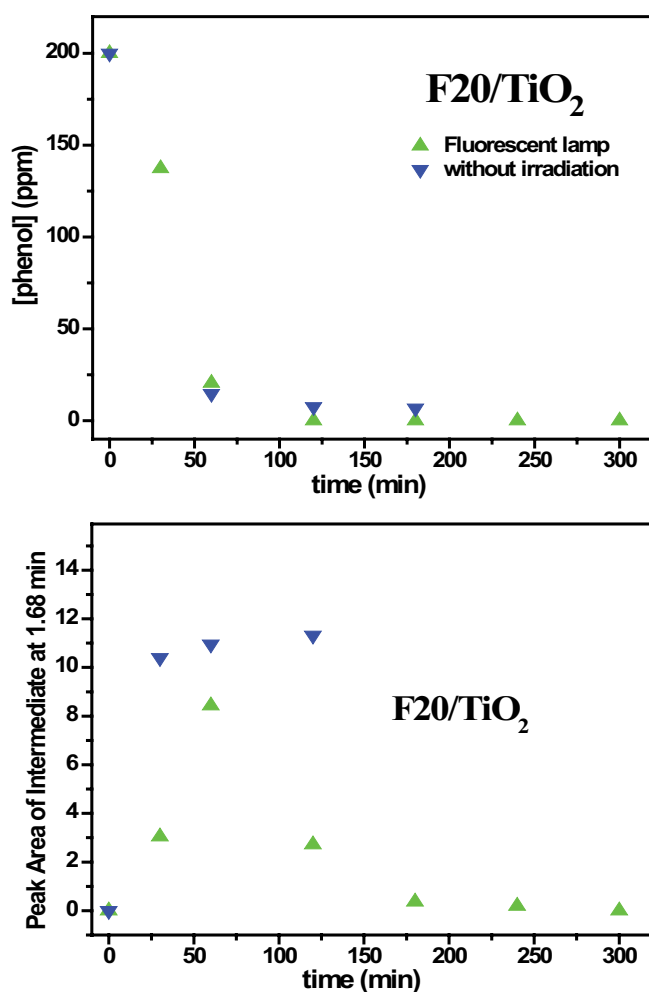

Fig. 6. Progress of degradation reaction with and without irradiation: 400 mL reaction solution with $[phenol]_o$ = 200 ppm and $[H_2O_2]_o$ = 0.0374 M, 0.25 g $F20/TiO_2$ catalyst, T = 30°C and jacketed 23 W fluorescence lamp in the case of irradiation.

However, the disappearance of phenol should not be considered as the only factor to evaluate the activity of used catalysts. This is because the degradation of phenol is a complex reaction with a series of steps that end up, upon complete oxidation (total mineralization), with CO_2. It is therefore important to evaluate how far the degradation process approaches total mineralization. Unfortunately, this point is missing in most literature reports on the heterogeneous Fenton-like degradation of organic pollutants. Fig. 6 shows how the area of degradation intermediates that appear in the HPLC chromatogram at a retention time of 1.68 min (a collection of intermediates that could not be separated and identified) changes over time. As expected for intermediates in consecutive reactions, it goes through a maximum. The fast decay of this maximum reflects how fast the intermediates undergo degradation. Intermediates are more rapidly degraded in the case of $F20/TiO_2$ than with any other catalyst investigated in this work (Fig. S1) suggesting the superiority of this system. The intermediates profile in Fig. 6 for $F20/TiO_2$ reflects also how significant irradiation with the fluorescent lamp can be. The catalytic performance is strongly enhanced by irradiation as evident by the disappearance of the intermediates at t_R = 1.68 min after 3 h of reaction. The COD value of final solution was thereby less than 3.5 mg O_2/L, confirming the occurrence of almost total mineralization. For the sake of comparison, it is worth noting that F16-V10/TiO_2 also achieved under irradiation a 100%-conversion of phenol in 120 min, the intermediates were, however, not efficiently degraded and a final COD value of 65 mg O_2/L after 5 h of reaction was observed. A similar behavior was observed for TiO_2 where the phenol concentration decreased by 90% after 5 h of reaction under irradiation, the intermediates amount was thereby found to grow monotonically throughout the reaction without reaching a maximum, ending with a COD value of 165 mg O_2/L.

The performance of the other catalytic systems in the Fenton's degradation of phenol is shown in Fig. S1. TiO_2, V10/TiO_2 and F16-V10/TiO_2 where completely inactive in the absence of irradiation. In general, adding vanadium to the $F20/TiO_2$ catalyst worsen its performance. Without irradiation, the V-containing systems are rather inactive. Under irradiation, the profile for intermediate degradation becomes broader indicating slow intermediate formation and subsequent degradation. The low efficiency of the V-rich systems (F20-V15/TiO_2 and F20-V25/TiO_2) is believed to be correlated with the formation of the vanadate phases which are believed to bind the copper and iron ions in the system and transform them into a less active form.

The catalyst recyclability is an important aspect to take in account when real application is considered. The $F20/TiO_2$ catalyst was hence tested for recyclability. The phenol degradation was investigated over 0.20 g $F20/TiO_2$ in 4 consecutive runs, between which the catalyst was separated by centrifugation, and re-used further in the next run without washing. The efficiency of phenol degradation is presented in Fig. 7 which shows that the phenol degradation efficiency in the fourth run decreased only down to 97% in comparison to 100% in the first run. Moreover, the area of degradation intermediates that appear in the HPLC chromatogram at a retention time of 1.68 min didn't change

significantly from run to run. This result suggests that the catalyst activity is retained and that it can be used several times without significant loss in activity. Accompanying metal leaching was also measured by means of atomic absorption spectroscopy. The final solution after the first run was found to contain 0.9 ppm iron and 2.2 ppm copper while after the 4th run it contained about 1.0 ppm iron and 2.5 ppm copper.

Fig. 8 represents the area of the intermediates at t_R = 1.68 min and the COD of the resulting solution after 5 h of reaction under irradiation with the fluorescent lamp. A good linear relationship is observed up to a COD value of 170 mg O_2/L. The area of the intermediates at t_R = 1.68 min can thus be used to estimate how far full mineralization is, without the need to perform the tedious COD measurements.

The application of Fe(III)/TiO_2 as a Fenton photocatalyst has been reported in literature. Yang et al. [23] presented a nanocomposite with TiO_2 nanoparticles on reduced graphene oxide-encapsulated Fe_3O_4 spheres as a highly efficient heterogeneous catalyst for the photo-Fenton
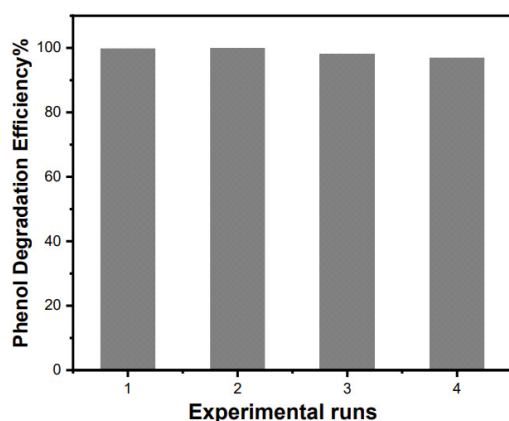

Fig. 7. Recyclability of the F20/TiO_2 catalyst: 400 mL reaction solution with [phenol]$_o$ = 200 ppm and [H_2O_2]$_o$ = 0.0374 M, 0.25 g catalyst, jacketed 23 W fluorescence lamp for 2 h.
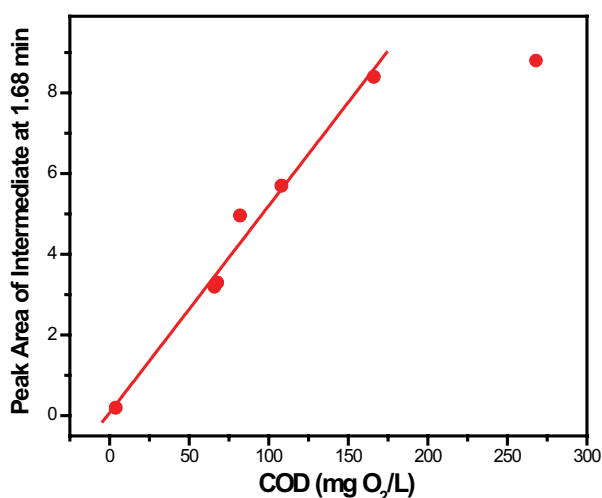

Fig. 8. Correlation between the area of the intermediates at t_R = 1.68 min and COD.

degradation of recalcitrant pollutants under neutral pH. The mentioned catalyst achieves for an initial H_2O_2 concentration of 0.044 M about 65% methylene blue degradation efficiency in 120 min, and that for an initial methylene blue concentration of only 10 ppm. The catalyst showed a much better performance than Fe_3O_4 alone [23]. In comparison, our F20/TiO_2 achieves almost 100% degradation of phenol in 100 min and that for an initial phenol concentration of 200 ppm. It is thereby to emphasize by the study of Yang et al. [23] the fate of the intermediates has not been monitored and the degradation efficiency is judged based only on the remaining concentration of methylene blue. On contrary, the fate of intermediates was monitored in this work where almost total mineralization of a 200 ppm phenol solution has been achieved on F20/TiO_2 in 180 min ending with a final COD value of 3.5 mg O_2/L.

The excellent degradation efficiency of F20/TiO_2 is manifested further by the relatively low catalyst-to-pollutant ratio applied in this study (3.1 mg$_{catalyst}$/mg$_{phenol}$). This is much smaller than values reported in literature for efficient photocatalysts (20 mg$_{catalyst}$/mg$_{methylene\ blue}$ [24], 20 mg$_{catalyst}$/mg$_{4-nitrophenol}$ [25], 80 mg$_{catalyst}$/mg$_{Rhodamine\ B}$ [26], 40 mg$_{catalyst}$/mg$_{phenol}$ [27], 25 mg$_{catalyst}$/mg$_{methylene\ blue}$ [28], 15 mg$_{catalyst}$/mg$_{methylene\ blue}$ [23]). Alqassem et al. [29], a ratio of 3.2 mg$_{catalyst}$/mg$_{phenol}$ has been applied for Co ferrite catalysts, the concentration of H_2O_2 was, however, 13 times larger than that used in this study.

Another important aspect of the excellent degradation efficiency of F20/TiO_2 is the low power of the visible light source used to accomplish total mineralization. In this work, a 23 W fluorescent lamp available in the market for normal lighting purposes was used. In literature, light sources with a much higher power were used, for example, 500 W tungsten lamp [24], 400 W metal-halide lamp [29], 300 W UV-Vis lamp [23] and 125 W fluorescent high-pressure mercury lamp [26]. Light sources with smaller power were also reported, for example, a 20 W fluorescent lamp [27], the degradation of the intermediates was not, however, monitored. Also, a 9 W UV-C low pressure mercury lamp was used [25]. This is, however, a UV-C lamp and the whole idea behind the application of visible-light source is to be able to replace the light source soon with solar irradiation. Indeed, the application of sunlight in the catalytic photodegradation of pollutants was reported [28], the concentration of H_2O_2 was 27 times larger than that used in this work.

3.4. Mechanism

The Fenton reaction is known to proceed over Fe-oxides and ferrites even in the dark. The oxides catalyze the decomposition of H_2O_2, producing thus .OH radicals which are, in turn, responsible for the oxidation of the pollutants.

$$Phenol + {}^{\bullet}OH \rightarrow CO_2 + H_2O \tag{2}$$

The reaction is photo-assisted as radiation of proper energy excites electrons from the valence band to the conduction band. The produced electrons facilitate the decomposition of H_2O_2 and the holes oxidize the hydroxide ions [11]. In both cases, hydroxyl radicals are produced. It is thereby important to notice that no photolytic decomposition

of H_2O_2 occurs as it requires wavelengths shorter than 320 nm [30], which are absent in the emission spectrum of the light source used in this work.

$$H_2O_2 + e^- \rightarrow {}^\bullet OH + OH^- \tag{3}$$

$$OH^- + h^+ \rightarrow {}^\bullet OH \tag{4}$$
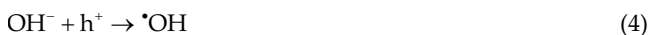
Bare TiO_2 by itself is not expected to contribute to the proposed photo-assisted Fenton reaction since it has a band gap energy of 3.2 eV corresponding to UV radiation shorter than 385 nm. However, when Fe^{3+} and Cu^{2+} become incorporated, the band gap is reduced to about 2.0 eV corresponding to wavelengths shorter than 620 nm, opening the door for the utilization of solar energy in the Fenton treatment of organic pollutants in wastewater.

4. Conclusions

In our attempts to develop a solid catalyst to degrade organic pollutants in wastewater via the Fenton-like reaction, vanadium-modified titania-supported CuO-Fe_2O_3 systems were investigated. Best performance has been observed for $F20/TiO_2$ that works well without irradiation, but its efficiency is highly enhanced under irradiation with 23 W fluorescent lamp achieving almost complete mineralization reducing thus the COD value below 4 mg O_2/L within 5 h. The catalytic efficiency decreases with increasing vanadium percentage, most probably due to the formation of vanadate phases, as evidenced by XRD and infrared. Using the fluorescent lamp opens the door for more environmentally friendly approaches, it suggests that solar energy can be used instead of UV light sources.

Acknowledgement

References

[1] X.D. He, P. Li, Surface water pollution in the Middle Chinese Loess Plateau with special focus on hexavalent chromium (Cr^{6+}): occurrence, sources and health risks, Exposure Health, 12 (2020) 385–401.

[2] N.Y. Donkadokula, A.K. Kola, I. Naz, D. Saroj, A review on advanced physico-chemical and biological textile dye wastewater treatment techniques, Rev. Environ. Sci. Biotechnol., 19 (2020) 543–560.

[3] Y. Deng, R. Zhao, Advanced oxidation processes (AOPs) in wastewater treatment, Curr. Pollut. Rep., 1 (2015) 167–176.

[4] E. Neyens, J. Baeyens, A review of classic Fenton's peroxidation as an advanced oxidation technique, J. Hazard. Mater., 98 (2003) 33–50.

[5] T.L.P. Dantas, V.P. Mendonça, H.J. José, A.E. Rodrigues, R.F.P.M. Moreira, Treatment of textile wastewater by heterogeneous Fenton process using a new composite Fe_2O_3/carbon, Chem. Eng. J., 118 (2006) 77–82.

[6] E. Casbeer, V.K. Sharma, X.-Z. Li, Synthesis and photocatalytic activity of ferrites under visible light: a review, Sep. Purif. Technol., 87 (2012) 1–14.

[7] G.H. Du, Z.L. Liu, X. Xia, Q. Chu, S.M. Zhang, Characterization and application of Fe_3O_4/SiO_2 nanocomposites, J. Sol-Gel Sci. Technol., 39 (2006) 285–291.

[8] J. Wu, X. Wang, H. Kang, J. Zhang, C. Yang, $CuFe_2O_4$ as heterogeneous catalyst in degradation of p-nitrophenol with photoelectron-Fenton-like process, Int. J. Environ. Sci. Technol., 71 (2014) 534–545.

[9] C.K. Cheng, Z.Y. Kong, M.R. Khan, Photocatalytic-Fenton degradation of glycerol solution over visible light-responsive $CuFe_2O_4$, Water Air Soil Pollut., 226 (2015) 1–12, doi: 10.1007/s11270-015-2592-2.

[10] N. Hamdan, M. Abu Haija, F. Banat, A. Eskhan, Heterogeneous catalytic degradation of phenol by a Fenton-type reaction using copper ferrites ($CuFe_2O_4$), Desal. Water Treat., 69 (2017) 268–283.

[11] A. Khan, Z. Valicsek, O. Horváth, Synthesis, characterization and application of Iron(II) doped copper ferrites ($Cu^{II}_{(x)}Fe^{II}_{(1-x)}Fe^{III}O_4$) as novel heterogeneous photo-Fenton catalysts, Nanomaterials, 10 (2020) 1–17, doi: 10.3390/nano10050921.

[12] G.-T. Pan, M.-H. Lai, R.-C. Juang, T.-W. Chung, T.C.-K. Yang, Preparation of visible-light-driven silver vanadates by a microwave-assisted hydrothermal method for the photodegradation of volatile organic vapors, Ind. Eng. Chem. Res., 50 (2011) 2807–2814.

[13] T.T. Alhmoud, S.S. Mahmoud, A.Y. Hammoudeh, Fenton-like degradation of phenol catalyzed by a series of fe-containing mixed oxides systems, IOP Conf. Ser.: Mater. Sci. Eng., 305 (2018) 012018.

[14] R. Ghanem, Preparation and Characterization of Supported Copper Ferrite Catalysts and their efficiency in the Fenton-Like Degradation of Phenol in Aqueous Solutions, Master Thesis, Yarmouk University, 2018.

[15] D.A.H. Hanaor, C.C. Sorrell, Review of the anatase to rutile phase transformation, J. Mater. Sci., 46 (2011) 855–874.

[16] R. Gonzalez, R. Zallen, Infrared reflectivity and lattice fundamentals in anatase TiO_2, Phys. Rev. B: Condens. Matter, 55 (1997) 7014–7017.

[17] M. Ocatia, V. Fornfis, J. Garcia Ramos, C. Serna, Factors affecting the infrared and Raman spectra of rutile powders, J. Solid State Chem., 75 (1988) 364–372.

[18] V. Sivakumar, R. Suresh, K. Giribabu, R. Manigandan, S. Munusamy, S. Praveen Kumar, S. Muthamizh, V. Narayanan, Copper vanadate nanoparticles: synthesis, characterization and its electrochemical sensing property, J. Mater. Sci.: Mater. Electron., 25 (2014) 1485–1491.

[19] M. Pelaez, N. Nolan, S. Pillai, M. Seery, P. Falaras, A. Kontos, P. Dunlop, J. Hamilton, J. Byrne, K. Shea, M. Entezari, D. Dionysiou, A review on the visible light active titanium dioxide photocatalysts for environmental applications, Appl. Catal., B, 125 (2012) 331–349.

[20] J. Tauc, R. Grigorovic, A. Vancu, Optical properties and electronic structure of amorphous germanium, Phys. Stat. Sol., 15 (1966) 627–636.

[21] M.I. Litter, M.A. Blesa, Photodissolution of iron oxides. IV. A comparative study on the photodissolution of hematite, magnetite, and maghemite in EDTA media, Can. J. Chem., 70 (1992) 2502–2510.

[22] N.R. Dhineshbabu, N. Nithyavathy, R. Vetumperumal, Study of structural and optical properties of cupric oxide nanoparticles, Appl. Nanosci., 6 (2016) 933–939.

[23] X. Yang, W. Chen, J. Huang, Y. Zhou, Y. Zhu, C. Li, Rapid degradation of methylene blue in a novel heterogeneous Fe_3O_4@rGO@TiO_2-catalyzed photo-Fenton system, Sci. Rep., 5 (2015) 1–10.

[24] P. Ajithkumar, S. Mohana, S. Sumathi, Synthesis, characterization, optical and photocatalytic activity of yttrium and copper co-doped zinc ferrite under visible light, J. Mater. Sci.: Mater. Electron., 31 (2020) 1168–1182.

[25] L.A. Frolova, O.V. Khmelenko, The study of Co-Ni-Mn ferrites for the catalytic decomposition of 4-nitrophenol, Catal. Lett., 53 (2020) 1–12.

[26] G. Wei, Y. Yang, Y. Li, L. Zhang, Z. Xin, Z. Li, L. Huang, A new catalytic composite of bentonite-based bismuth ferrites with good response to visible light for photo-Fenton reaction: application performance and catalytic mechanism, Appl. Clay Sci., 184 (2020) 1–8.

[27] M.F. Hanafi, N. Sapawe, The potential of ZrO₂ catalyst toward degradation of dyes and phenolic compound, Mater. Today, 19 (2019) 1524–1528.

[28] A.J.R. Luciano, L. de Sousa Soletti, M.E.C. Ferreira, L.F. Cusioli, M.B. de Andrade, R. Bergamasco, N.U. Yamaguchi, Manganese ferrite dispersed over graphene sand composite for methylene blue photocatalytic degradation, J. Environ. Chem. Eng., 8 (2020) 1–9.

[29] B. Alqassem, I. Othman, M. Abu Haija, F. Banat, Comparative catalytic activity of pure, mixed and P-modified CoFe₂O₄ nanoparticles for water treatment at neutral pH, Catal. Commun., 150 (2021) 1–19.

[30] B. Finlayson-Pitts, J. Pitts Jr., Chemistry of the Upper and Lower Atmosphere, California, 2000.
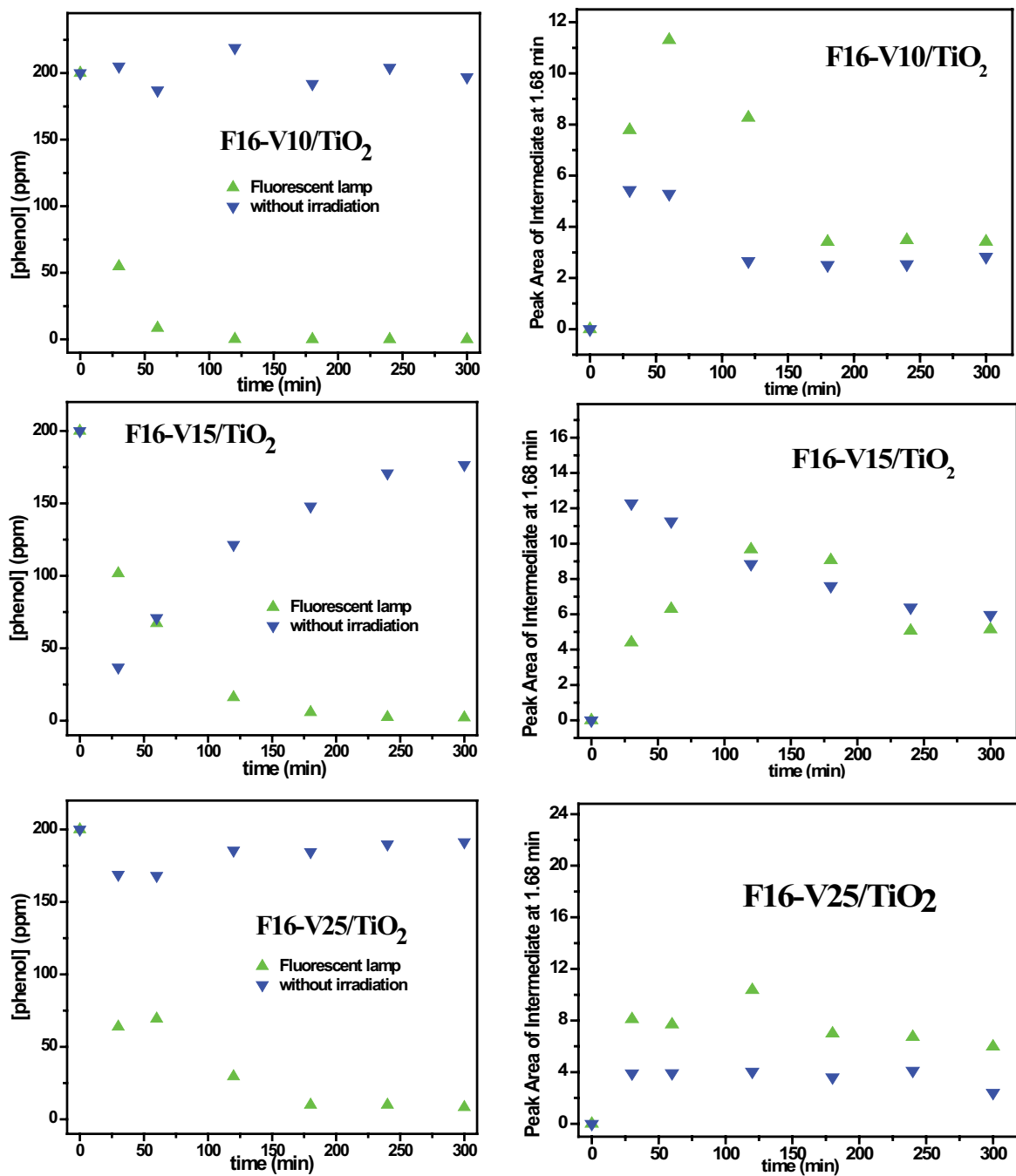
Supplementary information
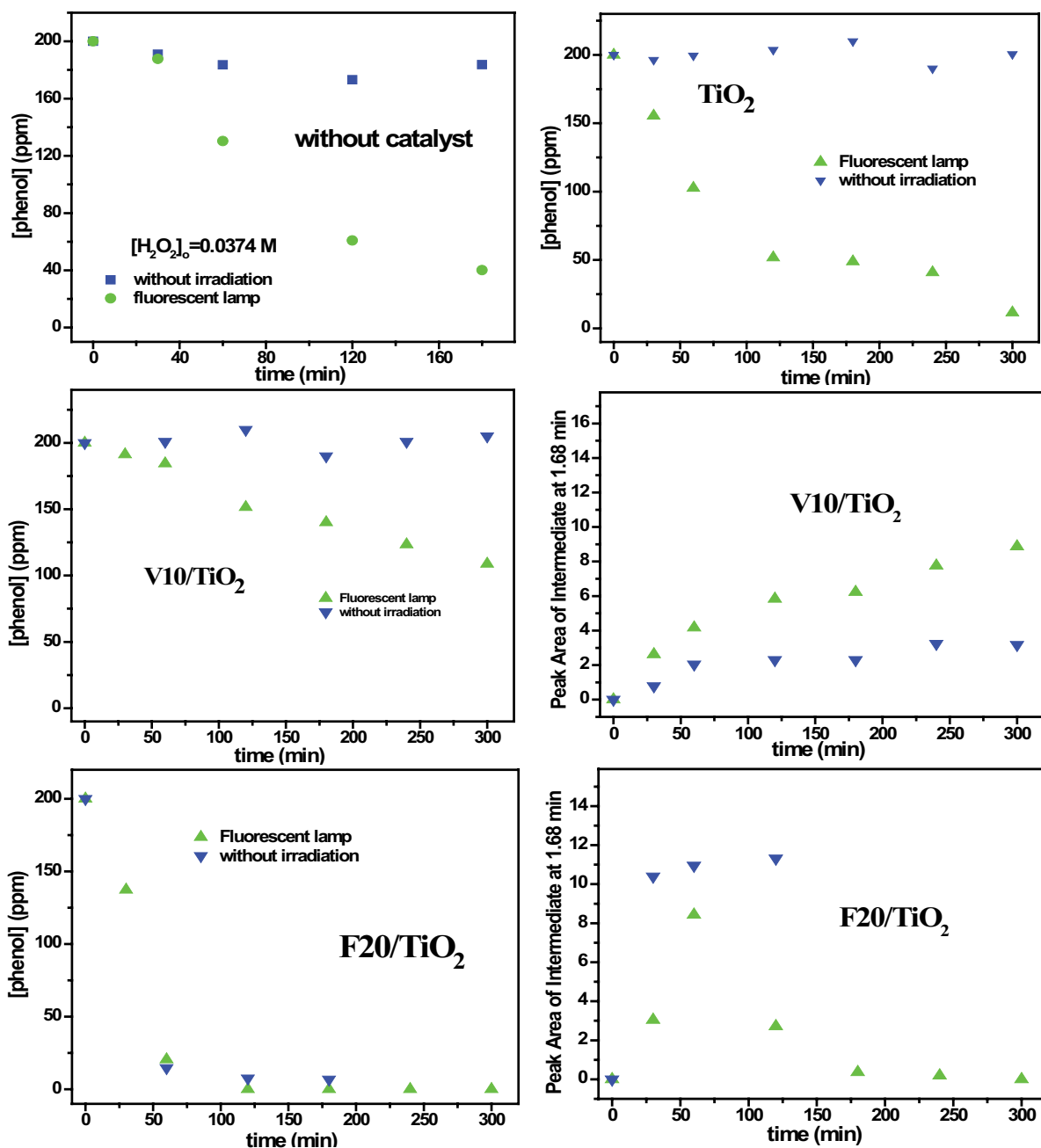
(*Continued*)

Fig. S1. Progress of degradation reaction with and without irradiation: 400 mL reaction solution with $[\text{phenol}]_o = 200$ ppm and $[\text{H}_2\text{O}_2]_o = 0.0374$ M, 0.25 g F20/TiO$_2$ catalyst, $T = 30°$C and jacketed 23W fluorescence lamp in case of irradiation.